Article

CaO-SiO$_2$-B$_2$O$_3$ Glass as a Sealant for Solid Oxide Fuel Cells

Andrey O. Zhigachev *, Ekaterina A. Agarkova, Danila V. Matveev and Sergey I. Bredikhin

The Institute of Solid State Physics of the Russian Academy of Sciences, 142432 Chernogolovka, Russia
* Correspondence: zhigachev@issp.ac.ru

Abstract: Solid oxide fuel cells (SOFCs) are promising devices for electrical power generation from hydrogen or hydrocarbon fuels. The paper reports our study of CaO-SiO$_2$-B$_2$O$_3$ material with composition 36 mol.% SiO$_2$, 26 mol.% B$_2$O$_3$, and 38 mol.% CaO as a high-temperature sealant for SOFCs with an operating temperature of 850 °C. The material was studied as an alternative to presently existing commercial glass and glass-ceramics sealants for SOFCs with operating temperature of 850 °C. Many of these sealants have limited adhesion to the surface of Crofer 22APU steel, commonly used in these SOFCs. The present study included X-ray diffraction, dilatometric, thermal, and microstructural analysis The study has shown that the softening point of the CaO-SiO$_2$-B$_2$O$_3$ glass is around 900 °C, allowing sealing of the SOFCs with this glass at convenient temperature of 925 °C. The CaO-SiO$_2$-B$_2$O$_3$ glass sealant has shown excellent adhesion to the surface of Crofer 22APU steel; SEM images demonstrated evidences of chemical reaction and formation of strong interface on sealant–steel contact surface. Furthermore, the glass has shown a coefficient of thermal expansion about 8.4×10^{-6} 1/K after sealing, making it thermomechanically compatible with the existing SOFC materials.

Keywords: glass; glass-ceramic; microstructure; sealant; SOFC

1. Introduction

Solid oxide fuel cells (SOFCs) are promising electrochemical devices for conversion of chemical energy of hydrogen and hydrocarbon fuels into electricity. The energy conversion process goes directly through electrochemical reactions, bypassing the fuel-burning stage. Compatibility of SOFCs with conventional hydrocarbon fuels along with high efficiency and nearly noiseless operation make them an attractive solution for industrial and domestic power generation.

SOFCs owe their compatibility with hydrocarbon fuels to their high operation temperatures; most of the commercial SOFC systems work at 800–100 °C. It should be noted that in the last two decades, active research on SOFCs operating at intermediate (600–800 °C) or low temperatures (500–600 °C) has been conducted [1,2], but these systems have not yet reached the commercialization level. High temperatures used in SOFCs not only allow use of hydrocarbon fuels, but also lead to high-quality exhaust heat that can be used for domestic or industrial heating. Unfortunately, high the operating temperature of SOFCs has its drawbacks. It increases duration of startup and stopping of SOFCs, introduces additional requirements to thermomechanical and chemical compatibility of the materials used in SOFCs, and complicates the choice of sealing materials for SOFCs [3].

Primary functions of the sealing materials in SOFCs include dividing fuel and air streams inside the fuel cell, isolating the internal gases flow from the environment, and mechanical consolidation of separate cells into a battery. No organic-based seals can be used at 800–1000 °C, so glasses and glass-ceramics are employed instead. Choice of sealants for SOFCs is a complicated task because they should meet a number of requirements. A sealant should have a coefficient of thermal expansion (CTE) close to that of both ceramic membrane (electrolyte) and metal interconnect (usually high-chromium steel or CFY alloy), typically in the $8–12 \times 10^{-6}$ 1/K range. In addition, a strong adhesion should exist between

a sealant and steel interconnect to ensure both impermeability for gas products and high mechanical strength of the battery. The last requirement for SOFC sealing materials is the stability of their chemical composition and physical properties during the operation of the battery.

A number of glass and glass-ceramic sealant compositions for SOFCs are reported in the literature and implemented in commercial products. Among the most frequently used chemical compositions, one may note the following:

1. Barium aluminosilicate glass-ceramics. Their approximate chemical composition is 45–55 mol.% SiO_2, 5–15 mol.% B_2O_3, 20–30 mol.% BaO, 5–15 mol.% Al_2O_3, minor amounts of ZrO_2, NiO, ZnO, and Cr_2O_3, and some other oxides. These glass-ceramics usually have CTE of 10.5–11 $\times$ 10^{-6} 1/K, nicely matching CTE of SDC and ScSZ electrolytes. They show decent adhesion to heat-resistant steel such as Crofer 22 APU [4–10]. In these glass-ceramics, the choice of the appropriate amount of flux is crucial to obtain material with the desired softening and glass-transition temperature.

2. Diopside-based glass-ceramics. These glass-ceramics are also frequently used to seal SOFCs. Approximate chemical composition is 15–20 mol.% CaO, 25–35 mol.% MgO, and 45–50 mol.% Al_2O_3, and minor quantities of Al_2O_3, SiO_2, and B_2O_3 [6,11,12]. These sealants also have CTE of about 10 $\times$ 10^{-6} 1/K and decent adhesion to conventional metal interconnect.

3. Modified soda–lime glass. Soda–lime glass, with the addition of alumina and increased calcia content, is sometimes considered as glass sealant for SOFCs [4]. An example of composition used is 50–60 % mol.% SiO_2, 5–10 mol.% Al_2O_3, 24–28 mol.% CaO, and 10–14 mol.% Na_2O.

The materials mentioned above, especially barium aluminosilicate glass-ceramics, provide good sealing in SOFCs according to the literature. The procedure of SOFC sealing with these materials includes heating of the whole battery well-above its operating temperature. For example, for batteries operating at 850 °C, typical sealing temperature is 950 °C (Schott 394 glass). Dwell at the elevated temperature usually takes a few hours if conventional sealants are used so that reaction between the sealant and metal interconnect takes place and a strong interface is formed. The dwell at elevated temperatures may cause undesirable changes in the structure of electrodes due to sintering processes and may lower power output of the cell.

It is thus desirable to use glass or glass-ceramic sealant that quickly reacts with the material of a bipolar plate forming strong interface such that it remains stable under operating conditions. Indeed, other requirements for sealants still hold true for such sealants. They should be thermomechanically compatible with high-chromium steel or CFY and with the electrolyte used in the cell. Their properties should not deteriorate during the operation of the fuel cell through crystallization or through further reaction with either steel or the gas environment.

In the present work, we have investigated the glass-ceramic sealant of CaO-SiO_2-B_2O_3 system with high boron oxide content of 26 mol.% B_2O_3. This system was chosen because calcium borosilicate glasses are known to have CTE in the range 8–10 $\times$ 10^{-6} 1/K and glass-transition temperature about 650–700 °C [13–16]. CaO-SiO_2-B_2O_3 glasses with boron oxide content above 7–8 wt. % are rarely used as sealants for SOFCs; they primarily find applications in the sealing of microelectronic components working at near-room temperature [17–19]. The main reason for the limited high-temperature use of these glasses is volatility of boron oxide in glasses and its ability to cause poisoning of the cathode materials when volatilized [20,21]. However, in the present research, we hoped to achieve a high degree of crystallization of the sealant material after heat treatment to bind the boron oxide into the crystal lattice and into reaction products with steel and thus, lower boron mobility.

The main aims of the study were the following:

1. Study interface between $CaO-SiO_2-B_2O_3$ sealant and Crofer 22 metal interconnect after brief heat treatment or after treatment at temperatures lower than are conventionally used;
2. investigate thermomechanical compatibility of the $CaO-SiO_2-B_2O_3$ sealant and Crofer 22 interconnects;
3. investigate degree of crystallinity and phase composition of the sealant after the sealing procedure both in and out of contact with steel interconnect.

2. Materials and Methods

We prepared a sealant with chemical composition 38 mol.% CaO, 26 mol.% B_2O_3, and 36 mol.% SiO_2. Choice of the composition was based on the previous publications on low-temperature applications of $CaO-B_2O_3-SiO_2$ seals [13]. As initial materials for preparation of the sealant, we used >99 % pure calcium carbonate, boric acid, and silicon dioxide (Chemcraft, Russia). In order to mix the precursors homogeneously, we added bidistilled water and mixed the slurry with a laboratory mixer UED-20 (UED Group, Russia) for 5 min. The slurry was then left to dry in a laboratory oven at 100 °C for 15 h to remove water.

The dried mixture was then placed into platinum crucible and heated in air to 1500 °C at heating rate of 2.5 °C/min. Heating was conducted in a vertical load furnace LHT 02/17 LB (Nabertherm, Germany). We chose low heating rate to allow full decomposition of precursors to take place before the melting. We held the melt at 1500 °C for 1 h for the components to form homogeneous melt. Then, we quenched the melt into bidistilled water. After cooling of the water, we extracted the pieces of the resulting material and dried them at 100 °C for 2 h.

The dried pieces of the material were ground with a mechanical mortar Pulverisette 2 (Fritsch, Germany). We used zirconia pestle and mortar to minimize contamination of the material during grinding. We estimated the size of the ground powder with laser diffraction method (Analysette 22 Next, Fritsch, Germany) and compared it to size of commercially available powder glass Schott 394. For the purpose of the measurement small quantity of ground powder was dispersed in bidistilled water, ultrasonicated to break any agglomerates, and subjected to static light scattering measurement. It was performed to ensure that there was no significant particle size difference that could influence comparison of properties of the materials.

We performed X-ray diffraction (XRD) analysis of as-prepared sealants after heat treatment both in and out of contact with Crofer 22 APU. XRD analysis was performed on finely ground powder with copper X-ray tube in Bragg–Brentano reflective geometry with Smartlab (Rigaku, Japan) diffractometer. Peaks were identified with the use of PDF database. The latter was used as a reference material of a bipolar plate. XRD data were used to estimate degree of crystallinity of the material and identify crystalline phases if any were present.

We investigated high-temperature behavior of the prepared material. For this purpose, we have put about 0.3 g of the studied material on Crofer 22 APU (ThyssenKruppVDM, Berlin, Germany) plate with dimension 20 × 20 × 2 mm. The powder formed a loose cone with 10-milimeter base and about 10-milimeter height. The plate with the powder was then put to furnace and heated to a maximum temperature of 850–950 °C at 2 °C/min rate, held there for 1 h, and cooled down at the same rate. Low heating and cooling rates were chosen to minimize effects caused by CTE mismatch. Plate with the sealant was then visually assessed to estimate suitable sealing temperature of the prepared material. We ground the sealant after high-temperature treatment to prepare fine powder and performed XRD analysis of its phase compositions. We also cut rectangular samples with approximate dimensions 3 × 1 × 1 mm from the heat-treated sealant and measured its CTE in air with dilatometer L75Vertical (LINSEIS, Berlin, Germany). The samples were measured with heating and cooling rates of 3 °C/min and were held at 850 °C for 2 h. Ends of the samples were covered with thin zirconia pellets to minimize reaction of the sealant with

the measurement chamber. Expansion of zirconia pellets was accounted for and subtracted from the final data.

In order to assess strength of the sealant adhesion to the Crofer 22 APU plate, we performed a mechanical test. The steel plate was fixed in a vertical position by a lower part not covered with the sealant in clamps. Then, we applied bending load to the upper part of the plate in a way such that the sealant/steel interface was under tensile stress. We registered the applied load at which delamination of the sealant occurred and calculated the corresponding flexural stress.

We also investigated microstructure of sealant/steel interface. To prepare samples for this study, we deposited a hollow square pattern of sealant on $20 \times 20 \times 2$ mm Crofer 22 APU plate. For the deposition of the sealant, we used F4200N (Fisnar, Copenhagen, Denmark) dispenser with terpineol-glass-PVB paste. Organic components for the paste were supplied by Chemcraft, Russia. The as-deposited sealant was dried and covered on top with similar Crofer plate. This "sandwich" structure was loaded with a force of approximately 1 N and heat-treated in a furnace on the described above routine. A 150-micrometer zirconia delimiter was put in the center of the assembly to avoid leaking of the sealant under the load at elevated temperature. After cooling of the assembly, we prepared and polished cross-sections of the assembly. We prepared SEM images of the cross-sections with Supra 50 VP (Carl Zeiss, Germany) microscope. Both our material and commercial Schott 394 glass were investigated this way. We used energy-dispersive X-ray spectroscopy (EDXS) for elemental analysis of the cross-section and sealant/steel interface.

Thermal cycling tests were conducted on "sandwich" assemblies after heat treatment at 925 °C. For thermal cycling, we put the assemblies with no load applied into a furnace and heated them to 850 °C (typical temperature of SOFCs operation) with 2 °C/min heating rate, held at this temperature for 2 h, and then cooled down to room temperature with 2 °C/min cooling rate.

Schematic diagram of the sequence of the experiments conducted in the present study is given for reference in Figure S1 (Supplementary Materials).

3. Results and Discussion

$CaO-SiO_2-B_2O_3$ sealant melted at 1500 °C flowed freely from the platinum crucible into water. Its viscosity, as assessed visually, was much lower than that of barium aluminosilicate, diopside, and modified soda–lime glass sealants melted at the same temperature. The as-quenched calcium borosilicate sealant was opaque white contrary to what we observed on other types of sealants, which were transparent.

Mechanical strength of the as-quenched $CaO-SiO_2-B_2O_3$ sealant was similar to that of other sealants as judged from time required to mill quenched chunks of the material into fine powder.

Particle size distribution of the $CaO-SiO_2-B_2O_3$ powder is presented in Figure 1 along with the data for commercial powder Schott 394 measured under the same conditions. It is clear from the presented particle size distribution that the prepared sealant was similar to the commercial product, although with slightly narrower distribution especially for larger particles. Peaks of the distribution for our sealant lie at ~1.5 μm and at ~10–12 μm. Commercial powder has a wider distribution slightly shifted toward larger particle size with the rightmost peak at 30–40 μm. It should be noted that this peak corresponding to 30–40 μm particle can also be observed on the powder of our sealant, but there the peak is much less intensive. The difference between the distributions can be illustrated by d_{10}, d_{50}, and d_{90} values of the presented data. The values are shown on the insert in Figure 1. All the values are slightly lower for the $CaO-SiO_2-B_2O_3$ sealant, indicating that its particle size distribution is shifted toward lower values. The most notable difference is in d_{90} value, which is predictable given the difference in the right part of the distributions.
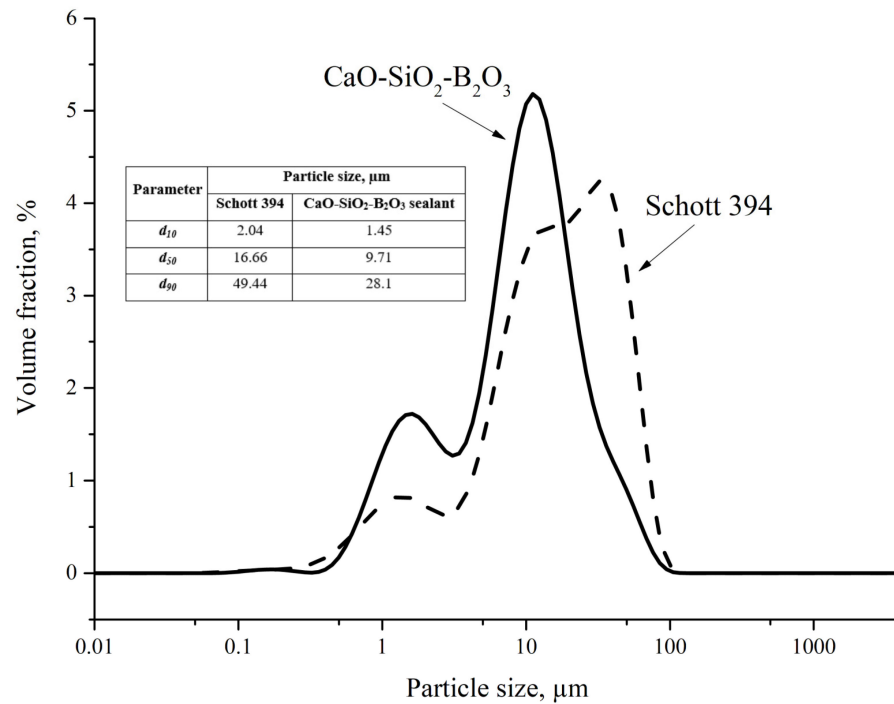
Figure 1. Particle size distribution in a ground powder of CaO-SiO$_2$-B$_2$O$_3$ sealant and in commercial Schott powder.

Figure 2 shows XRD pattern of the ground CaO-SiO$_2$-B$_2$O$_3$ sealant. No crystalline peaks can be seen; three broad amorphous halos are present instead. They correspond from left to right to interatomic distances 9.23 Å, 3.132 Å, and 2.01 Å. Among these distances, only 2.01 Å may be clearly attributed to B–O bond length [22]. Other distance cannot be attributed to either Si–O or Ca–O bond, which have lengths of 1.60–1.65 Å and 2.45–2.54 Å [23,24]. The low-angle peaks may correspond not to distances between adjacent atoms, but to distance between adjacent "strands" of the glass network.
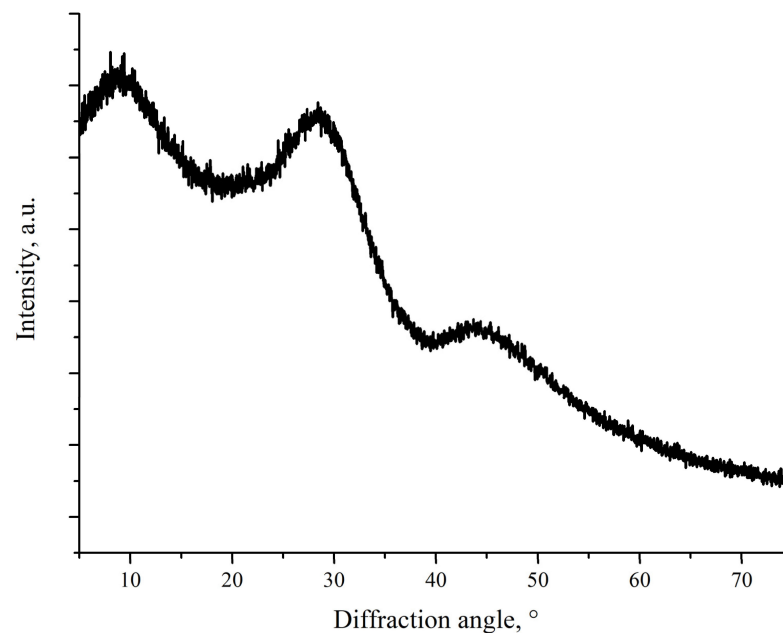
Figure 2. XRD pattern of as-quenched CaO-SiO$_2$-B$_2$O$_3$ sealant.

Figure 3 shows schematic depiction of the sealant-on-plate assembly after heat treatment at different temperatures for 1 h. We did not insert photographs here; because of the relatively small size of the samples, it was difficult to make a high-quality "macrophotograph", showing the necessary details. Colors used in the figure are nearly identical to actual colors of different zones of the sealant after heat treatment. The color of Crofer 22 APU plate is shown only schematically with hatching. Relative dimensions of the sealants and the steel plate are lifelike with factual size of the plate $20 \times 20 \times 2$ mm. Wetting angles are also shown true to life.
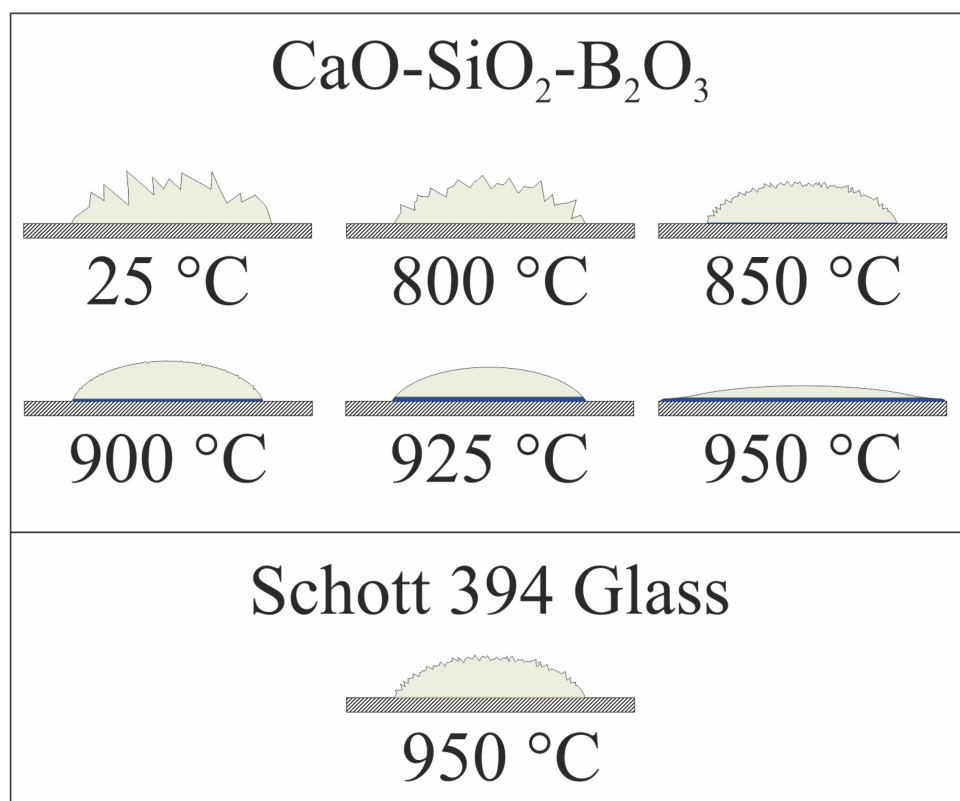

Figure 3. Shape and color of sealants after heat treatment for 1 h.

For $CaO-SiO_2-B_2O_3$ sealant, heat treatment at 800 °C for 1 h did not cause any notable change in the geometry of the powder pile. Sharp edges of the particles remained and the particles themselves were only loosely bound to each other. We observed no reaction zone on sealant/steel interface. Increase in the temperature to 850 °C led to some softening of the angles of the powder pile and to the formation of a thin (~ 100 um), but notable layer of dark blue color at the interface with steel. Even further increase in temperature led to progressive softening of the relief of the pile and thickening of the blue layer to ~300 μm at 925 °C. At this temperature, surface of the sealant became smooth, forming a drop, slightly wetting the steel plate. It indicates that the glass softening point lies between 850 °C and 925 °C. For samples heated to 950 °C, we observed spreading of the sealant over the surface of the plate, demonstrating excellent wetting and low viscosity of the sealant. The latter is undesirable for sealing of SOFCs because low-viscosity sealant may flow from the designed areas and block air or fuel channels. In the following discussions, part of the sealant that was not in direct contact with the steel plate and did not change color significantly is named "White area". The part that was in contact with the plate and changed its color to saturated blue is named "Blue area". The key difference between these regions is that the former represents change in the sealant itself after the heat treatment, while the latter represents products of interaction of the sealant and Crofer plate. Experiments with Schott 394 glass were conducted only for 950 °C because it is a recommended sealing temperature

for this sealant. The degree of the sealant softening at this temperature was similar to that of $CaO-SiO_2-B_2O_3$ sealant at 850 °C. Significant visual difference lies in the color of the contact layer on the interface with steel. The color is saturated yellow as opposed to the dark blue of $CaO-SiO_2-B_2O_3$.

Mechanical test of adhesion strength was performed on samples with $CaO-SiO_2-B_2O_3$ sealant heat-treated at 925 °C and on Schott 394 sealant heat-treated at 950 °C. We registered the bending load was applied when the delamination of the sealant from the steel plate took place. In the case of Schott 394, sealant delamination occurred at a load of 11 N, which corresponded to flexural stress of 0.12 MPa. In the case of $CaO-SiO_2-B_2O_3$, delamination of the sealant took place at a load of 28 N, corresponding to flexural stress of 0.31 MPa. In the present experiment setup, flexural stress represents tensile stress at steel-sealant interface in the interface plane; therefore, it can be said that the strength of the $CaO-SiO_2-B_2O_3$ adhesion to steel surface is approximately 2.5 times higher than that of Schott 394 sealant. It should be noted that during exfoliation of the studied sealant, it came of the steel surface with significant starting velocity unlike what was observed on the Schott 394 sealant. Such behavior may follow from both external mechanical stresses introduced during the test and from thermomechanical stresses generated at sealant–steel interface due to possible CTE mismatch. Since it is likely that the appearance of the blue zone on the sealant/steel interface was a result of the reaction between the $CaO-SiO_2-B_2O_3$ sealant and steel, we performed XRD study of both white and blue areas of the sealant after heat treatment at 925 °C. Figure 4 shows XRD patterns for both of these areas.
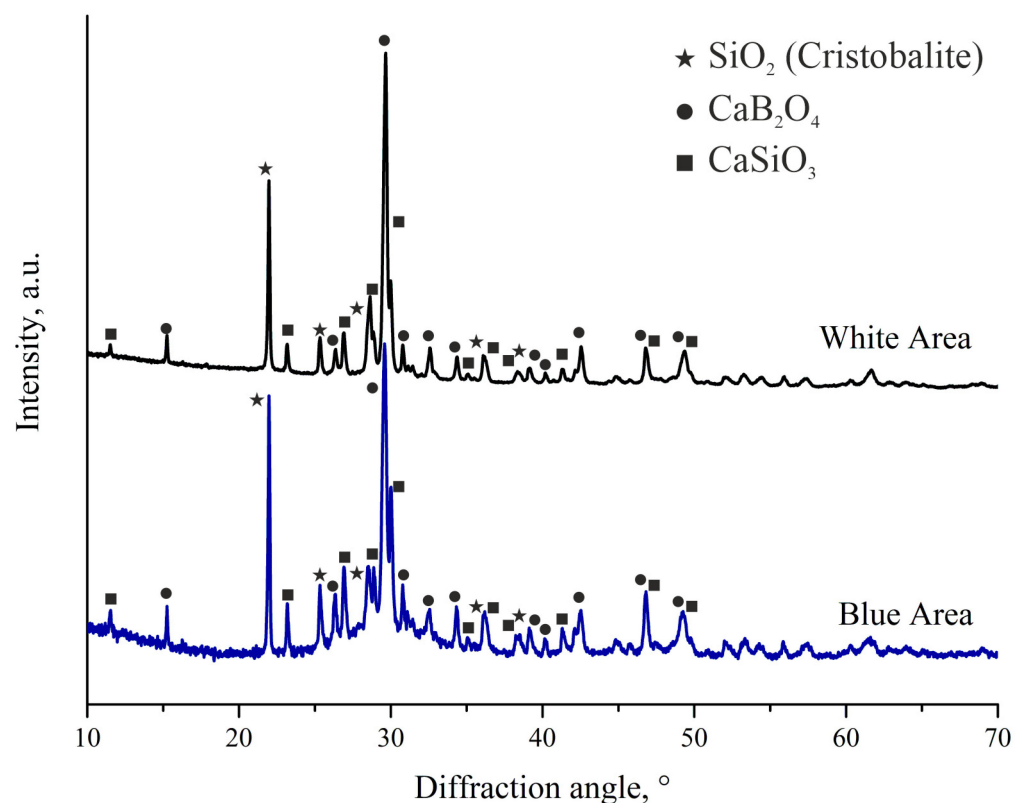
Figure 4. XRD patterns of white and blue areas of the $CaO-SiO_2-B_2O_3$ after heat treatment at 925 °C. Symbols mark positions of the most intensive peaks of different phases.

Sealant that was not in contact in Crofer plate is fully crystallized (upper curve in Figure 4). The most prominent crystalline phases attributed to the observed peaks are CaB_2O_4 (PDF 00-032-0155), SiO_2 (Cristobalite modification, PDF 00-039-1425), and $CaSiO_3$ (PDF 00-043-1460). The amount of amorphous phase in the white area is negligible. The ratio between $CaSiO_3$ and CaB_2O_4 allowed us to estimate boron content in the heat-treated

sealant; it turned out to be close to the nominal value. XRD pattern of the blue area shows the same crystalline phases with similar molar fractions of the phases with a slightly higher $CaSiO_3/CaB_2O_4$ ratio, which may serve as an indication that part of boron oxide took part in reaction with the steel plate. The products of the reaction are likely to be amorphous, as evidenced by the appearance of an amorphous halo on the XRD pattern. We detected no crystalline phases containing iron or chromium (main components of Crofer 22 APU steel) in the blue area. However, the coloration itself hints at the presence of Cr^{3+} ions in the interface area. It may be assumed, thus, that the amorphous phase is formed through reaction of at least boron oxide and components of the steel plate. Of course, other components of the sealant could take part in the formation of the amorphous layers. XRD patterns show that the sealant after heat treatment is glass-ceramic in the area near the bipolar plate. Taking into account that thickness of the seal is usually well-below 500 μm, we may safely assume that the entire seal will be composed of the "blue" zone, meaning that the seal will be in the glass-ceramic state after the sealing procedure.

It was difficult to calculate molar fractions of the crystalline phases in powder prepared from the blue area because of the significant contribution of the amorphous phase. Roughly, ratios of the crystalline phases may be estimated to be 55 mol.% $CaSiO_3$, 30 mol.% CaB_2O_4, and 15 mol.% SiO_2. We managed to calculate the amount of amorphous phase only approximately to be 60–70% of total crystalline phases content. CTEs of the present phases are, according to the literature:

1. $CaSiO_3$ has a CTE of 11.2×10^{-6} 1/K in a wide range of temperatures, as calculated from high-temperature crystallographic data on $CaSiO_3$ reported in the literature [25].
2. We found no results on CTEs of CaB_2O_4 in the literature. The closest match we found in the literature is a paper by Kluev et al. [26], where the authors reported CTE of glass consisting of 40 mol.% CaO and 60 mol.% B_2O_3 to be 7.29×10^{-6} 1/K in 20–300 °C range. Other results mentioned in the paper imply that material with 50 mol.% CaO and 50 mol.% B_2O_3 may have slightly higher CTE.
3. SiO_2 in β-cristobalite has a CTE changing significantly with temperature, having CTE of 10.9×10^{-6} 1/K at 100–500 °C rapidly falling to 1.7×10^{-6} 1/K in 500–1000 °C [27].

Among the present crystalline phases, cristobalite, predictably, has the lowest average CTE in the 100–850 °C range. It means that cristobality may serve as a main source of thermomechanical stresses on the sealant-interconnect interface, which may be somewhat mitigated by the glassy phase presenting dampening CTE mismatch. Crystallization of SiO_2 is an undesirable process, lowering overall CTE of the sealant and causing internal thermomechanical stresses. This process should be suppressed by the introduction of additional components to the sealant. We plan to use them in the process of further development of the reported sealant.

To assess thermomechanical compatibility of the sealant and Crofer 22 APU, we cut a rectangular sample of the sealant after heat treatment at 925 °C. We managed to prepare suitable samples from the white area of the treated sealant because the blue area was too thin (<300 μm). Of course, in the case of SOFCs sealing, the sealing space will be filled with the material with phase composition of the blue area because of typically low thickness of the seal (usually well-below 500 μm). Nonetheless, dilatometric data obtained on the white (Figure 5) area may give a useful insight into properties of the blue area because of the closeness of their phase composition.

It should be noted that the data presented in Figure 5, obtained on the sealant after heat treatment, does not illustrate properties of the original glass. Instead, it shows properties of the sealant after the sealing procedure, which, we believe, are more important when studying thermomechanical compatibility of the sealant and steel. Average CTE in range 400–850 °C is 8.4×10^{-6} 1/K. This value is lower than CTE of Crofer 22 APU ($11–12 \times 10^{-6}$ at 800–900 °C) and than that of zirconia electrolyte ($10.5–11 \times 10^{-6}$ 1/K). CTE of the CaO-SiO_2-B_2O_3 sealant is close to that of Schott 394 glass—8.6×10^{-6} 1/K. It allows us to assume that a sealant with CTE equal to 8.4×10^{-6} 1/K is thermomechanically compatible with Crofer 22 APU and zirconia-based electrolytes. Since the data were

obtained on the sealant crystallized after heat treatment, it is impossible to determine the glass-transition temperature from the presented dilatometry data.
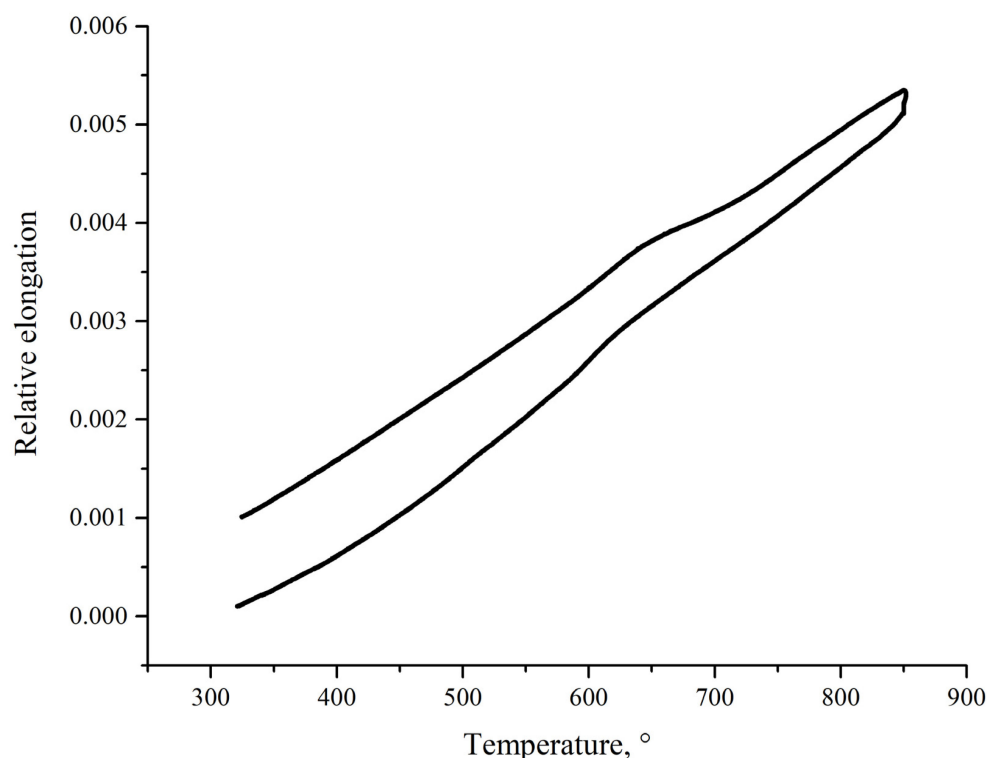

Figure 5. Dilatometric curve of the CaO-SiO$_2$-B$_2$O$_3$ sealant after heat treatment at 925 °C.

SEM images of the steel–sealant–steel assembly cross-sections are presented in Figure 6. Figure 6a,b features an assembly with the CaO-SiO$_2$-B$_2$O$_3$ sealant. It can be seen that a strongly pronounced interaction area is formed; it consists of elongated formations with predominant orientation normally to the interface surface. The interaction area appears consistently along the entire sealant–steel contact surface. The sealant layer all along the studied surface showed a solid structure without cracks or extensive pore networks, which could lead to the loss of impermeability of the material. We have also held some samples at the operation temperature of 850 °C for 100 h to examine if the reaction zone propagates further into the sealant. We found no evidence of such behavior; SEM images of as-heat-treated and aged samples were hard to distinguish from each other.

In the assembly with Schott 394, the interaction area was not pronounced, as can be seen in Figure 6c. SEM images of the assembly with Schott 394 sealant show regions where delamination of the sealant from steel surface is observed (central part of the lower interface in Figure 6c). The delamination might have taken place due to possible factors: (a) poor adhesion combined with thermal stresses at the interface or (b) contamination of the steel plate surface prior to sealant deposition. The latter is unlikely because of the careful preparation of the samples and consistency of the appearance of the areas with delamination, but it cannot be entirely ruled out.

The reported CTE of the sealant is lower than that of steel interconnect or zirconia electrolyte. The CTE mismatch causes thermomechanical stress, which was not high enough to lead to immediate delamination of the sealant, according to conducted mechanical tests. It, however, may lead to the degradation of the interface upon thermal cycling. SOFCs rarely undergo a high number of thermal cycles to room temperature, since they usually operate at a nearly constant temperature for prolonged periods. Nevertheless, a sealant-interconnect interface should withstand a small number of cycles inevitably occurring at startups or stops of the SOFC battery. We have thermally cycled the steel-sealant–steel assembly 20 times and after that obtained an SEM image of the polished cross-section. We

have observed no delamination or cracking of the sealant after 20 cycles. It may be supposed that CTE of the reaction zone (blue zone) is different from that of the bulk sealant, perhaps having intermediate value between bulk sealant and steel interconnect, thus avoiding generation of large amounts of thermomechanical stress on the interface. However, it is only an assumption, since we were not able to prepare a sample for dilatometry from the reaction zone because of its small size. Another possible assumption, which is indirectly supported by the SEM images of the interface, is that adhesion on the interface is strong enough to withstand the thermomechanical stress.
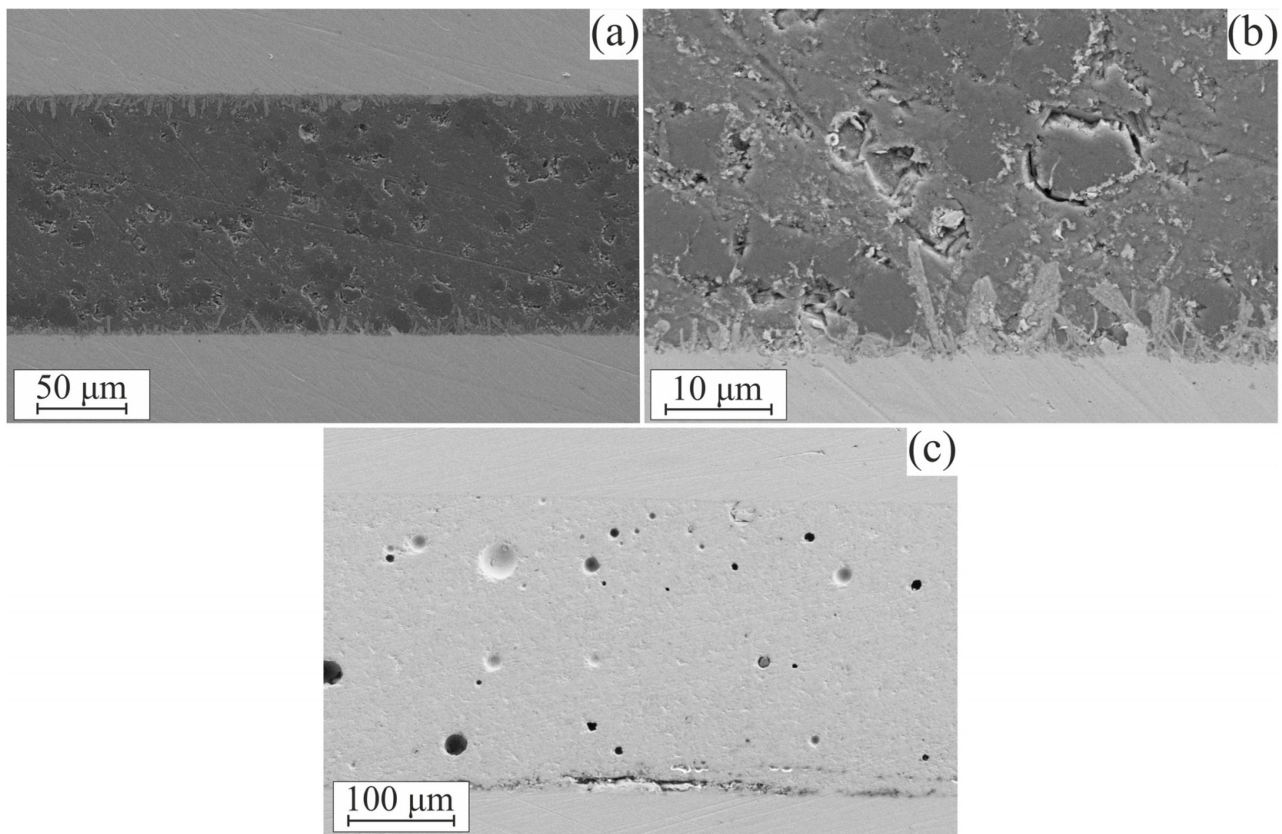
Figure 6. SEM images of the cross-sections of sealant–steel assembly: (**a**) CaO-SiO_2-B_2O_3 sealant, (**b**) close-up image of CaO-SiO_2-B_2O_3 sealant–steel interface, and (**c**) Schott 394 sealant.

For EDXS analysis of the sealant–steel assembly, we intentionally performed heat treatment of the assembly at 925 °C for 6 h instead of 1 h. The purpose of such treatment was to grow the sealant–steel interaction zone to obtain more reliable data on the elemental composition. Prolonged exposure to high temperatures caused intensive growth of the interaction zone with dendrite formations growing deep into the sealant layer. Figure 7 shows points where elemental composition was measured; these points are: (a) large dendrite formations originating at sealant–steel interface, (b) dark contrast regions in the sealant, and (c) gray-contrast areas in the bulk of the sealant. Table 1 summarizes our findings on the compositions in these points. It should be noted that EDXS does not allow detection of boron so boron is not listed in the table, but is indeed present as evidenced by XRD data (Figure 4).
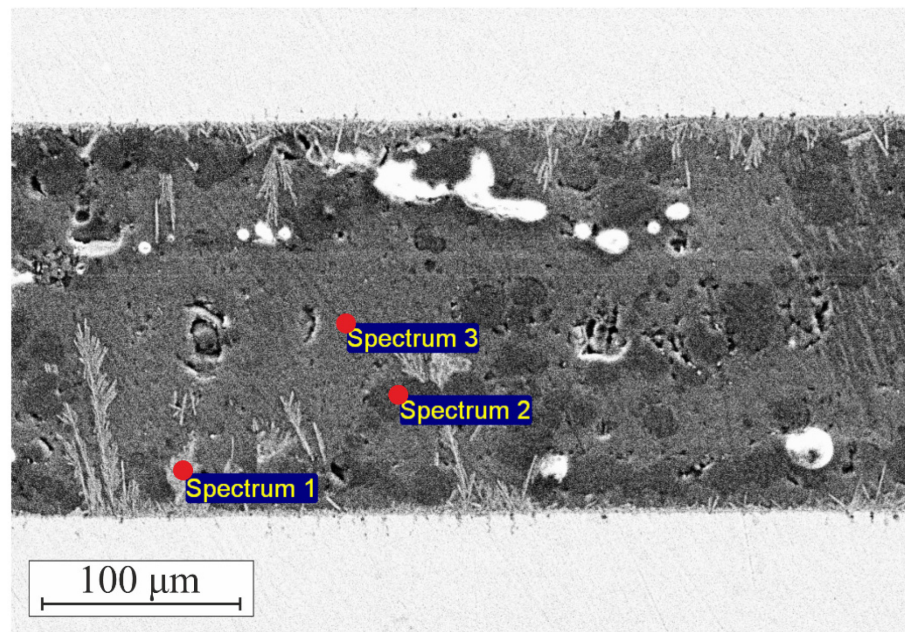
Figure 7. Choice of points for EDXS of heat-treated sealant–steel assembly.

Table 1. Elemental composition in the points shown in Figure 7.

Type of Atom	Content, mol.%		
	Point 1	Point 2	Point 3
Si	11.89	35.26	9.29
Ca	2.24	0.74	23.60
Cr	26.35	-	0.84
Fe	0.40	-	0.32
O	59.12	64.00	65.94

The gray-contrast area (point 3 in Figure 7) contains mostly Ca, Si, and O with minor quantities of Cr and Fe. Presented in Table 1, elemental composition in the point cannot be attributed to either $CaSiO_3$, SiO_2, or their mixture because of Ca/Si and Ca/O ratios. It is evident that the disbalance in the amount of the elements is due to the presence of the CaB_2O_4 phase. Darker contrast regions (point 2) show almost purely SiO_2 with some minor amounts of $CaSiO_3$. Dendrite formations at the interface contain large amounts of Cr and Si with a little Ca. It shows that at the sealant–steel interface, the sealant predominantly reacts with Cr. The ratios Cr/Si and Cr/Ca allow us to safely assume that the reaction product contains significant amounts of B. The latter was expectable because of the high reactivity of boron. Furthermore, it agrees with the observations made from XRD patterns of the reaction zone.

The main observed shortcoming of the studied sealant is its relatively low CTE of 8.4×10^{-6} 1/K, which is lower than CTEs of most materials used in SOFC. For example, metal interconnects and zirconia electrolytes usually have a CTE of about 11×10^{-6} 1/K. CTE of the studied sealant is also low relatively to CTEs usually offered by reported sealants. For example, barium aluminosilicate sealants often have CTEs of $8.5–14 \times 10^{-6}$ [4,9]. Calcium aluminosilicates may have CTEs in a wide range including $7–12 \times 10^{-6}$ 1/K, depending on the composition with higher values of CTE observed at low-silica and high-calcia contents [28]. Despite this difference in CTEs, it is close to that of commercially supplied sealants for SOFC, e.g., Schott 394 glass designed for high-temperature SOFCs has a CTE of 8.6×10^{-6}. Low CTE of the studied sealant is likely caused by the presence of cristobalite and calcium metaborate phases with low CTE. It may be possible to improve

thermomechanical properties of the sealant by substituting part of CaO for SrO or by introducing some additional components such as La_2O_3 [4].

It should be noted that we only managed to measure CTE of the heat-treated sealant that was not in contact with the steel interconnect. According to our XRD data, the part that was in contact with the interconnect contained a significant amount of glassy phase with some dissolved Cr^{3+} ions, as evidenced by EDXS data and by coloration of the reaction zone. This glassy phase likely has CTE intermediate between that of heat-treated sealant and steel interconnect, as indirectly evidenced by SEM images showing no cracks at the cross-section of steel–sealant assembly.

The glass-transition temperature of the prepared sealant was not measured, but it can be estimated from the literature data to be around 650–700 °C [17–19]. A high content of glassy phase after sealing along with a relatively low glass-transition temperature and excellent adhesion to the metal interconnect surface suggest that the prepared sealant may be suitable for the sealing of SOFCs with an operation temperature of 800–850 °C.

4. Conclusions

The $CaO\text{-}SiO_2\text{-}B_2O_3$ sealant prepared in the study may be considered a promising glass-ceramic sealant for SOFCs with an operation temperature of about 800–850 °C. It has excellent adhesion to the surface of Crofer 22 APU steel frequently used as a material of bipolar plates in SOFCs. The prepared sealant has an acceptable CTE of 8.4×10^{-6} 1/K comparable to that of commercial sealants, although significantly lower than that of the most SOFC sealants reported in the literature.

SEM images of the sealant-interconnect interface demonstrate that reaction took place between the components' forming layer, providing strong adhesion at the interface. In addition, the sealant formed a dense structure with no cracks or pore clusters, which indicates that this sealant can be used to prepare airtight seals for SOFCs. An excellent adhesive layer was formed after sealing at 925 °C for 1 h. Usually, the sealing of SOFCs operating at 850 °C requires heating to at least 950 °C for a few hours. The ability of the studied sealant to adhere strongly at relatively mild sealing conditions is beneficial for the preservation of the electrodes structure during sealing. Short-term aging at an operation temperature of 850 °C for 100 h caused no visible change in the morphology of the interface, indicating that the formed reaction zone is relatively stable.

We would like to note, however, that the 100-h experiment gives only preliminary information about the stability of the sealant–steel interface and that of the sealant itself. Further experiments with longer exposures should be carried out. A study of the sealant stability in humid environments at operation temperatures will be of particular interest. Furhtermore, experiments studying long-term stability of SOFCs sealed with the proposed sealants should be conducted. These experiments will allow for assessing the effect of high boron oxide content on electrode poisoning and studying stability of dielectric and thermomechanical properties of the sealant.

Data Availability Statement: Not applicable.

Conflicts of Interest: The authors declare no conflict of interest.

References

1. Kaur, G. *Intermediate Temperature Solid Oxide Fuel Cells: Electrolytes, Electrodes and Interconnects*; Elsevier Science: Amsterdam, The Netherlands, 2019.
2. Shao, Z.; Tadé, M.O. *Intermediate-Temperature Solid Oxide Fuel Cells*; Springer: Luxembourg, 2016.
3. Tietz, F. Thermal expansion of SOFC materials. *Ionics* **1999**, *5*, 129–139. [CrossRef]
4. Singh, K.; Walia, T. Review on silicate and borosilicate-based glass sealants and their interaction with components of solid oxide fuel cell. *Int. J. Energy Res.* **2021**, *45*, 20559–20582. [CrossRef]
5. Sohn, S.-B.; Choi, S.-Y.; Kim, G.-H.; Song, H.-S.; Kim, G.-D. Stable sealing glass for planar solid oxide fuel cell, J. *Non. Cryst. Solids* **2002**, *297*, 103–112. [CrossRef]
6. Fergus, J.W. Sealants for solid oxide fuel cells, J. *Power Sources* **2005**, *147*, 46–57. [CrossRef]
7. Ghosh, S.; Kundu, P.; Das Sharma, A.; Basu, R.N.; Maiti, H.S. Microstructure and property evaluation of barium aluminosilicate glass–ceramic sealant for anode-supported solid oxide fuel cell. *J. Eur. Ceram. Soc.* **2008**, *28*, 69–76. [CrossRef]
8. Meinhardt, K.D.; Kim, D.-S.; Chou, Y.-S.; Weil, K.S. Synthesis and properties of a barium aluminosilicate solid oxide fuel cell glass—Ceramic sealant. *J. Power Sources* **2008**, *182*, 188–196. [CrossRef]
9. Puig, J.; Ansart, F.; Lenormand, P.; Antoine, L.; Dailly, J. Sol-gel synthesis and characterization of barium (magnesium) aluminosilicate glass sealants for solid oxide fuel cells. *J. Non. Cryst. Solids* **2011**, *357*, 3490–3494. [CrossRef]
10. Kermani, P.S.; Ghatee, M.; Yazdani, A. Synthesis and Characterization of Barium Aluminosilicate Glass as the Sealant for Solid Oxide Fuel Cell Application. *Adv. Ceram. Prog.* **2020**, *6*, 25–30. [CrossRef]
11. Reddy, A.A.; Tulyaganov, D.U.; Pascual, M.J.; Kharton, V.V.; Tsipis, E.V.; Kolotygin, V.A.; Ferreira, J.M.F. Diopside–Ba disilicate glass–ceramic sealants for SOFCs: Enhanced adhesion and thermal stability by Sr for Ca substitution. *Int. J. Hydrogen Energy* **2013**, *38*, 3073–3086. [CrossRef]
12. Reddy, A.A.; Tulyaganov, D.U.; Goel, A.; Pascual, M.J.; Kharton, V.V.; Tsipis, E.V.; Ferreira, J.M.F. Diopside–Mg orthosilicate and diopside–Ba disilicate glass–ceramics for sealing applications in SOFC: Sintering and chemical interactions studies. *Int. J. Hydrog. Energy* **2012**, *37*, 12528–12539. [CrossRef]
13. Dai, B.; Zhu, H.; Zhou, H.; Xu, G.; Yue, Z. Sintering, crystallization and dielectric properties of CaO-B_2O_3-SiO_2 system glass ceramics. *J. Cent. South Univ.* **2012**, *19*, 2101–2106. [CrossRef]
14. Veron, E.; Garaga, M.N.; Pelloquin, D.; Cadars, S.; Suchomel, M.; Suard, E.; Massiot, D.; Montouillout, V.; Matzen, G.; Allix, M. Synthesis and structure determination of $CaSi_{1/3}B_{2/3}O_{8/3}$: A new calcium borosilicate. *Inorg. Chem.* **2013**, *52*, 4250–4258. [CrossRef] [PubMed]
15. Yan, T.; Zhang, W.; Mao, H.; Chen, X.; Bai, S. The effect of CaO/SiO_2 and B_2O_3 on the sintering contraction behaviors of CaO-B2O3-SiO2 glass-ceramics. *Int. J. Mod. Phys. B* **2019**, *33*, 1950070. [CrossRef]
16. Chang, C.-R.; Jean, J.-H. Crystallization kinetics and mechanism of low-dielectric, low-temperature, cofirable CaO-B_2O_3-SiO_2 glass-ceramics. *J. Am. Ceram. Soc.* **1999**, *82*, 1725–1732. [CrossRef]
17. Zhu, H.; Liu, M.; Zhou, H.; Li, L.; Lv, A. Study on properties of CaO-SiO_2-B_2O_3 system glass-ceramic. *Mater. Res. Bull.* **2007**, *42*, 1137–1144. [CrossRef]
18. Shao, H.; Wang, T.; Zhang, Q. Preparation and properties of CaO–SiO_2–B_2O_3 glass-ceramic at low temperature. *J. Alloys Compd.* **2009**, *484*, 2–5. [CrossRef]
19. Chiang, C.-C.; Wang, S.-F.; Wang, Y.-R.; Wei, W.-C.J. Densification and microwave dielectric properties of CaO–B_2O_3–SiO_2 system glass–ceramics. *Ceram. Int.* **2008**, *34*, 599–604. [CrossRef]
20. Rodríguez-López, S.; Haanappel, V.A.C.; Durán, A.; Muñoz, F.; Mather, G.C.; Pascual, M.J.; Gross-Barsnick, S.M. Glass–ceramic seals in the system MgO-BaO-B_2O_3-SiO_2 operating under simulated SOFC conditions. *Int. J. Hydrog. Energy* **2016**, *41*, 15335–15345. [CrossRef]
21. Zhang, T.; Fahrenholtz, W.G.; Reis, S.T.; Brow, R.K. Borate volatility from SOFC sealing glasses. *J. Am. Ceram. Soc.* **2008**, *91*, 2564–2569. [CrossRef]
22. Inoue, H.; Aoki, N.; Yasui, I. Molecular dynamics simulation of the structure of borate glasses. *J. Am. Ceram. Soc.* **1987**, *70*, 622–627. [CrossRef]
23. Henderson, G.S. A Si K-edge EXAFS/XANES study of sodium silicate glasses. *J. Non. Cryst. Solids* **1995**, *183*, 43–50. [CrossRef]
24. Mastelaro, V.R.; Zanotto, E.D.; Lequeux, N.; Cortès, R. Relationship between short-range order and ease of nucleation in $Na_2Ca_2Si_3O_9$, $CaSiO_3$ and $PbSiO_3$ glasses. *J. Non. Cryst. Solids* **2000**, *262*, 191–199. [CrossRef]
25. Swamy, V.; Dubrovinksy, L.S.; Tutti, F. High-temperature Raman spectra and thermal expansion of wollastonite. *J. Am. Ceram. Soc.* **1997**, *80*, 2237–2247. [CrossRef]
26. Klyuev, V.P.; Pevzner, B.Z. Thermal expansion and glass transition temperature of calcium borate and calcium aluminoborate glasses. *Glass Phys. Chem.* **2003**, *29*, 127–136. [CrossRef]
27. Aumento, F. Stability, lattice parameters, and thermal expansion of β-cristobalite. *Am. Miner.* **1966**, *51*, 1167–1176.
28. Shelby, J.E. Formation and properties of calcium aluminosilicate glasses. *J. Am. Ceram. Soc.* **1985**, *68*, 155–158. [CrossRef]